Solid State Ionics 262 (2014) 625–629

Contents lists available at ScienceDirect

Solid State Ionics

journal homepage: www.elsevier.com/locate/ssi

Oxygen vacancy redistribution in $PbZr_xTi_{1-x}O_3$ (PZT) under the influence of an electric field

G. Holzlechner *, D. Kastner, C. Slouka, H. Hutter, J. Fleig

Christian Doppler Laboratory of Ferroic Materials, Institute of Chemical Technologies and Analytics Vienna University of Technology, Vienna, Austria

ARTICLE INFO

Article history:
Received 16 May 2013
Received in revised form 21 August 2013
Accepted 25 August 2013
Available online 18 September 2013

Keywords:
Oxygen tracer diffusion
ToF-SIMS
Oxygen vacancy diffusion
Field-driven stoichiometry polarization
Resistance degradation
PZT

ABSTRACT

Oxygen isotope exchange experiments are performed in donor doped $PbZr_xTi_{1-x}O_3$ (PZT) under field load. A detailed mapping of the oxygen tracer ions and thus indirectly of the oxygen vacancy distribution is enabled by spatially resolved time-of-flight secondary ion mass spectrometry (ToF-SIMS). Hence, knowledge can be gained on the oxygen vacancy redistribution under the influence of high electric fields applied to Cu inner electrodes of a PZT multilayer stack. Upon field load an enhanced oxygen tracer concentration is measured near to the cathode and interpreted in terms of a field-driven oxygen vacancy accumulation at an oxide ion blocking Cu cathode. Oxygen tracer depth profiles in near-anode and near-cathode diffusion zones give quantitative information on local grain and grain boundary diffusion coefficients and their dependence on applied voltages.

1. Introduction

$PbZr_xTi_{1-x}O_3$ (PZT) based materials have become one of the most important electroceramics for applications such as electromechanical transducers, sensors and actuators [1,2]. To improve the performance of PZT based applications, a detailed understanding of field-driven degradation phenomena and their defect chemical background is essential. Oxygen vacancies are proposed to play an important role in fatigue and resistance degradation of PZT or other electroceramics [3–16]. However, quantitative information on the defect chemistry and oxygen transport properties of PZT under field load is still rudimentary. Among others, there is a lack of knowledge on how different electric fields or electrode materials and geometries affect the oxygen vacancy distribution and the corresponding oxygen tracer diffusivity. Moreover, it has to be clarified how far this may cause resistance degradation.

The aim of this study is thus to investigate the redistribution of oxygen vacancies in a multilayer PZT stack under the influence of different voltages (electric fields) applied to built-in Cu inner electrodes. During DC polarization the donor-doped PZT samples were exposed to an oxygen tracer-rich atmosphere. The oxygen tracer distribution was then analyzed by subsequent time-of-flight secondary ion mass spectrometry (ToF-SIMS). Since the resulting oxygen tracer diffusion coefficient depends on the vacancy concentration, a kind of mapping of the oxygen vacancy distribution became possible and indicates a field-driven stoichiometry polarization in PZT under field load.

2. Experimental

2.1. Sample preparation, ^{18}O diffusion experiment and DC polarization

The PZT samples were supplied by EPCOS OHG (A Member of TDK-EPC Corporation, Deutschlandsberg, Austria) and consist of 1.5 mol% Nd doped $PbZr_xTi_{1-x}O_3$ (PZT) with a composition close to the morphotropic phase boundary. PZT was sintered together with Cu inner electrodes (distance of ca. 70 μm) to a multilayer actuator stack [15]. Samples of ~$6 \times 3 \times 1$ mm^3 were cut from a part of the multilayer stack. The sample geometry and an image of a sample after polishing are shown in Fig. 1.

In the diffusion cell, two Cu inner electrodes were electrically contacted and due to a current collector on one side of the sample (see Fig. 1) two PZT layers were polarized simultaneously. Prior to tracer diffusion (and field load) the PZT samples were kept in ambient air for 20 min at the diffusion temperature of 500 °C. After this pre-annealing, the ambient atmosphere was changed to 200 mbar oxygen tracer partial pressure (Campro Scientific GmbH, 97.1 atm% $^{18}O_2$; 99.7 vol% chemical purity) and a voltage between 20 V and 75 V was applied. The samples were kept for 4 h under field load in the $^{18}O_2$ atmosphere and then, still under applied voltage, quenched to room temperature in $^{18}O_2$ atmosphere (<100 °C within 2 min). Within the times used here, conductivity changes at 500 °C were within a factor of two to

* Corresponding author.
E-mail address: gerald.holzlechner@tuwien.ac.at (G. Holzlechner).

0167-2738/$ – see front matter © 2013 Elsevier B.V. All rights reserved.
http://dx.doi.org/10.1016/j.ssi.2013.08.027

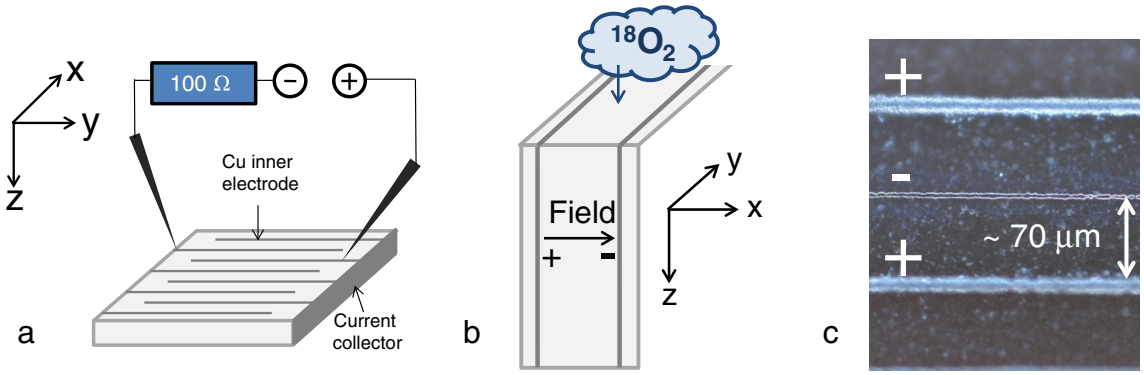

Fig. 1. a) Scheme of the PZT sample geometry and electrical measurements in $^{18}O_2$ atmosphere. b) Visualization of the direction of the applied field which is perpendicular to the measured tracer depth profiles. c) Optical microscopy image of the PZT surface after the diffusion experiment under field load.

three and pronounced resistance degradation did not take place. Details of conductivity changes are given elsewhere [17,18].

2.2. ToF-SIMS analysis and data quantification

All SIMS measurements were performed on a TOF.SIMS 5 instrument (ION-TOF, Münster, Germany) operating a bismuth primary ion gun (25 keV, Bi_1^+) in the "Collimated Burst Alignment" (CBA) mode. Adjustable primary ion currents in the CBA mode enable an optimization of ToF-SIMS analysis for oxygen isotope measurements to guarantee an accurate determination of the oxygen isotopic fraction [19,20].

The ^{18}O fraction f^*_{18O} is given by the experimentally obtained $^{16}O^-$ and $^{18}O^-$ secondary ion intensities (I_{16O}, I_{18O}) according to

$$f^*_{18O} = \frac{I_{18O} - I_{18O,bg}}{I_{16O} - I_{16O,bg} + I_{18O} - I_{18O,bg}}, \quad (1)$$

where $I_{16O,bg}$ and $I_{18O,bg}$ are the corrected background intensities near to the main ion mass peak. To obtain the bulk diffusion coefficient D_b, the solution of Fick's second law of diffusion [21]

$$f_{18O} = \frac{f^*_{18O} - f_{bg}}{f_{gas} - f_{bg}} = erfc\frac{z}{2\sqrt{D_b t}} - e^{hz + h^2 D_b t} \times erfc\left(\frac{z}{2\sqrt{D_b t}} + h\sqrt{D_b t}\right) \quad (2)$$

was fitted to the near-surface part of the tracer depth profiles. In Eq. (2) $h = k/D_b$, with k representing the surface exchange coefficient, z is the depth, t the annealing time, $f_{bg} = 2.05 \times 10^{-3}$ denotes the ^{18}O natural abundance and $f_{gas} = 0.971$ the isotope fraction of the annealing gas. Diffusion tails in some depth with severe deviations from Eq. (2) indicate existence of fast grain boundary diffusion. In such cases assumption of "type B" diffusion kinetics enables a quantification of the grain boundary diffusion using the solution given by Whipple [22] and Claire [23]. The grain boundary width is estimated by 3 nm, a typical value found in many perovskite type ceramics [24,25].

In general, the oxygen tracer diffusion coefficient D is given by the vacancy diffusion coefficient D_v, the oxygen vacancy concentration c_v (relative to the number of lattice sites) and the correlation factor f_c according to [26]

$$D = D_v * c_v * f_c. \quad (3)$$

Owing to this dependence of the oxygen tracer diffusion coefficient on the vacancy concentration, information on the oxygen vacancy distribution can be drawn from the spatial distribution of the tracer diffusion coefficient.

3. Analysis of the oxygen tracer diffusion in dependence of the voltage

First qualitative but very illustrative information can be gained from ^{18}O distribution images after the ^{18}O isotope exchange experiments with an electric field of 10.4 kVcm^{-1} (75 V) applied to the Cu inner electrodes for 4 h. The ^{18}O cross-section in Fig. 2(a) shows a typical depth distribution of the oxygen tracer obtained by integration in y-direction

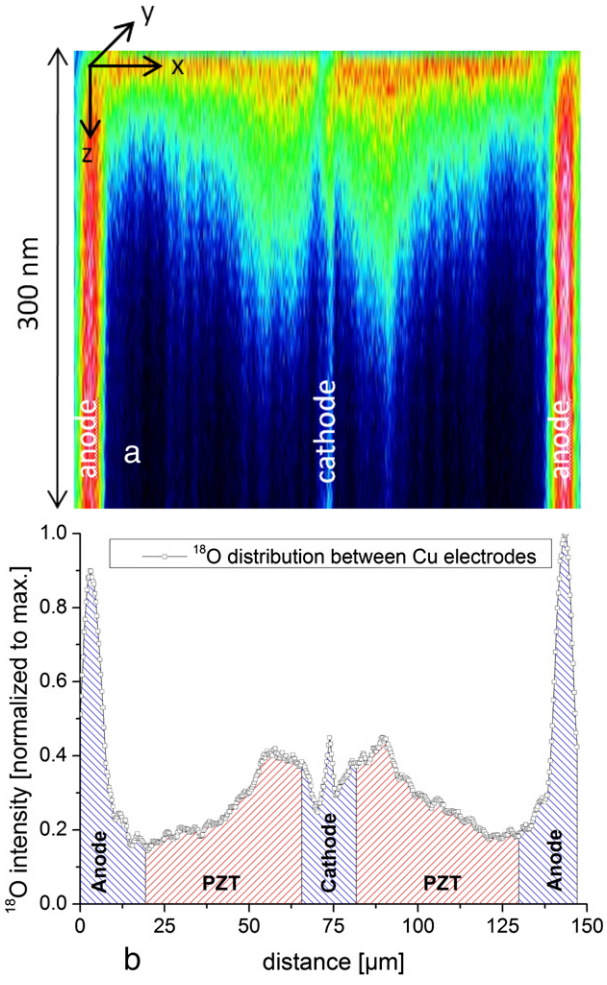

Fig. 2. ^{18}O tracer distributions resulting during field load of 10.4 kVcm^{-1} (75 V) at 500 °C for 4 h. a) Cross-section image of the ^{18}O diffusion zone after integration in y-direction, b) after further integrating the ^{18}O fraction profile in a depth of 200–300 nm.

(along the electrode plane, cf. Fig. 1). The penetration depth of the enhanced tracer fraction depends on the location; it is significantly larger in the near-cathode region. The profile in Fig. 2(b) results from integrating the ^{18}O signals in a depth of 200–300 nm. Again an enhanced oxygen tracer fraction can be observed near to the cathode, suggesting fast oxygen diffusion in this region. The very high tracer level in the anode can be attributed to oxidation of the Cu electrode at 500 °C annealing temperature (see below).

For further quantification of the voltage dependency of the oxygen diffusion, ^{18}O depth profiles were determined in morphologically homogeneous near-anode and near-cathode diffusion zones as well as in non-stressed areas. It should be emphasized that the electric field is perpendicular to the measured tracer profiles (Fig. 1b). Measurements with and without applied field show a diffusion profile that can be quantified by Eq. (2), see Fig. 4a. A tracer fraction of 2.92×10^{-3} (average value of the last ten ^{18}O fraction values) in 550 nm depth is obtained for the reference profile, and thus the ^{18}O natural abundance of $(2.05 \pm 0.14) \times 10^{-3}$ is not achieved, however, this is possibly caused by some residual porosity since an analysis in terms of grain boundary diffusion did not lead to meaningful results.

Compared to the depth profiles obtained without applied electric field, enhanced ^{18}O fractions were observed in field-stressed PZT in the near-cathode area already for a field load of 2.8 $kVcm^{-1}$ (20 V), see Fig. 3(a, b). Moreover, very pronounced diffusion tails appear under field load. The near-anode PZT area also exhibits a slightly enhanced tracer fraction compared to the reference measurement and a diffusion tail. Fig. 3(c, d) displays the depth profiles obtained from the tracer diffusion experiments with 10.4 $kVcm^{-1}$ (75 V). All general trends observed for the oxygen tracer distribution after 20 V load are found again and are even more pronounced for 75 V.

As described in Section 2.2 the first approximately 100 nm of all diffusion profiles could be quantified by Eq. (2) (cf. Fig. 4a) and thus a tracer bulk diffusion coefficient could be deduced. From ln $(f^*_{18O}) - z^{6/5}$ plots (cf. Fig. 4b) grain boundary diffusion coefficients D_{gb} were calculated. However, those should be taken as first estimates rather than exact values since there was partly some arbitrary act in choosing the region from which D_{gb} was analyzed. Moreover, indication of a time dependent change of the diffusion coefficients during field load was found by varying the diffusion time interval and further measurements are required to get more accurate values.

In near-anode PZT zones the bulk diffusion coefficients D_b of about $\sim 1 \times 10^{-15}$ cm^2s^{-1} indicate slightly faster oxygen tracer diffusion compared to the reference measurement without applied voltage ($D_b = 5.1 \times 10^{-16}$ cm^2s^{-1}, see Fig. 4). As expected from the similar diffusion profiles in Fig. 3, the bulk diffusion coefficients are very similar for all near-anode measurements, irrespective of the applied voltages. For near-cathode diffusion, however, a field-dependent oxygen tracer diffusion coefficient in PZT bulk material could be determined, showing faster ^{18}O diffusion for higher voltages. The near-cathode surface exchange coefficient k also increases with increasing voltage while in the near-anode region voltage independent k values are determined (cf. Table 1). Those values, however, should be taken with some care since the fit quality using Eq. (2) is not ideal near to the surface (cf. Fig. 4a).

Despite the problems mentioned above, some trends can still be concluded from the grain boundary diffusion coefficient – in addition to the fact that fast grain boundary diffusion only sets in under applied field (fast grain boundary diffusion in PZT without field was reported above 600 °C in Ref. [27]). First, D_{gb} values are about four orders of magnitude larger than D_b in the bulk. Second, for near-cathode oxygen tracer

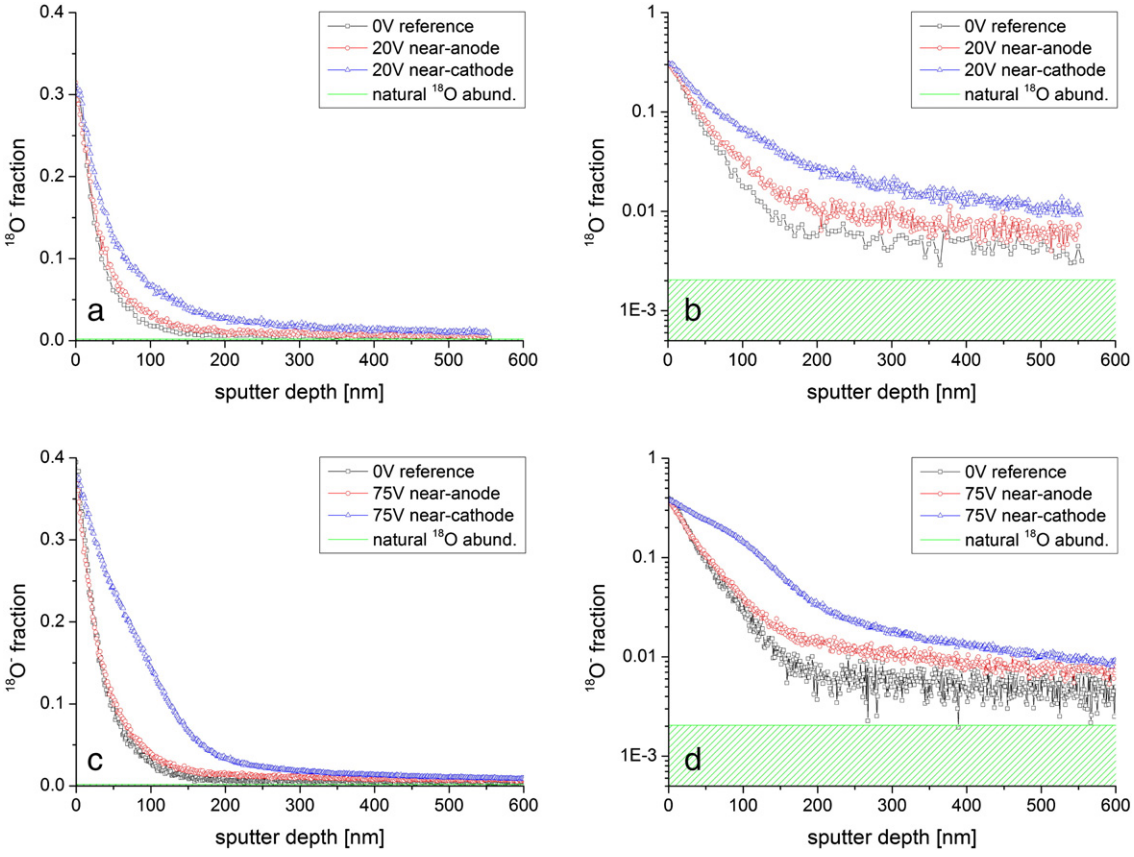

Fig. 3. ^{18}O depth profiles in near-anode and near-cathode diffusion zones or non-stressed reference areas without applied field. (a) and (b) shows the resulting linear and logarithmic plotted oxygen tracer diffusion profiles resulting under the influence of 20 V field load. The impact of 75 V DC polarization on the ^{18}O fractions is shown in (c) and (d).

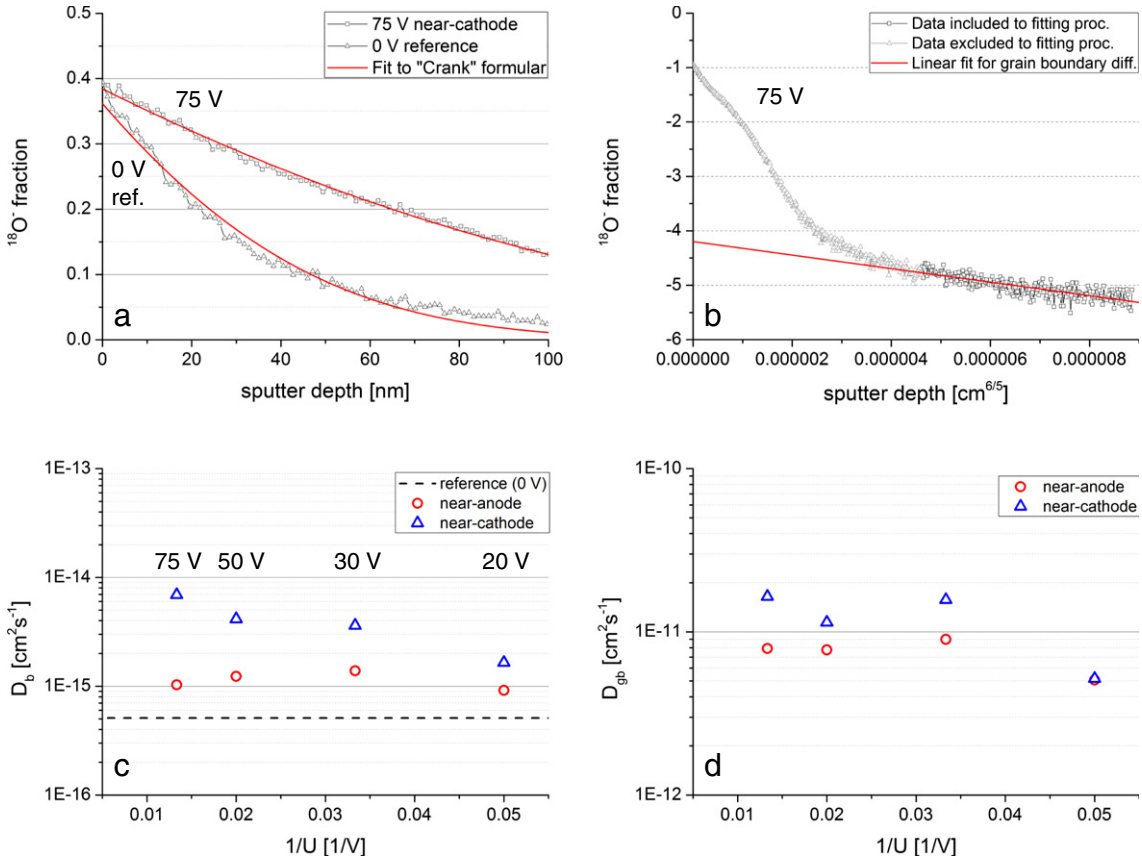

Fig. 4. Determination and voltage dependency of the oxygen tracer diffusion coefficients, showing in (a) the fit of the first 100 nm diffusion profile to the "Crank" formula to obtain D_b of a reference and a stressed PZT, in (b) the linear fit to the diffusion tail for gaining D_{gb}, in (c) the resulting PZT bulk diffusion coefficients D_b and in (d) the PZT grain boundary diffusion coefficients D_{gb}.

diffusion higher D_{gb} values are found compared to near-anode areas and for higher fields D_{gb} was larger than for the lowest voltage.

4. Discussion of the field-driven oxygen vacancy redistribution

According to Eq. (3) an increased tracer diffusion coefficient indicates an enhanced oxygen vacancy concentration, provided D_v remains constant. Hence, we conclude that upon field load a substantially enhanced oxygen vacancy concentration is present near to the cathode. Also close to the anode a slight increase is found. A redistribution of oxygen vacancies in an oxide is a well-known phenomenon and was analyzed in detail for acceptor-doped $SrTiO_3$ and $BaTiO_3$ [3,9]. A certain (low) level of oxygen vacancies also exists in donor-doped PZT [15,17,27,28] and for two oxide ion blocking electrodes, oxygen vacancy depletion in the near-anode region would be expected during DC polarization, while vacancies should accumulate close to the cathode.

The cathodic vacancy accumulation is in accordance with the measured D_b increase. Analysis of the near-anode depth profiles, however, also indicates a slightly enhanced ^{18}O fraction (Fig. 3) and higher D_b values (Fig. 4), i.e. a higher oxygen vacancy concentration. Therefore, the question arises whether the Cu inner electrodes are indeed oxide ion blocking. The optical microscopy image in Fig. 1(b) shows strong topological changes of the Cu anode which indicates anodic oxidation. This means that oxygen ions are consumed at the anode and hence oxygen vacancies are created under field load at 500 °C. The cathode, on the other hand, is regarded as more or less oxygen blocking with no supply of oxide ions and thus strong accumulation of oxygen vacancies takes place. This model can explain the slight enhancement of D_b (and thus of the vacancy concentration) near to the anode and the strong enhancement close to the cathode. However, absence of strong resistance changes on the same time scale indicates that resistance degradation of such samples has to be caused by different yet unknown processes.

5. Conclusion

The mapping of the oxygen tracer distribution under the influence of high fields shows a strong variation of the oxygen diffusivity between the field-loaded Cu inner electrodes of donor doped PZT. From ^{18}O depth profiles in near-cathode diffusion zones, substantially higher oxygen tracer diffusion coefficients than in non-stressed areas are determined and the values further increase with increasing field. This indicates a stoichiometry polarization of the PZT layer due to

Table 1
Calculated values of the surface exchange coefficients.

	20 V	30 V	50 V	75 V	Ref. (0 V)
Near-cathode (cm/s)	1.25×10^{-10}	2.46×10^{-10}	2.04×10^{-10}	3.49×10^{-10}	0.99×10^{-10}
Near-anode (cm/s)	1.12×10^{-10}	1.69×10^{-10}	1.44×10^{-10}	1.28×10^{-10}	

motion of oxygen vacancies towards an ion blocking Cu cathode. Also the near-anode region shows slightly higher ^{18}O fraction instead of lower ones expected for anodic oxygen vacancy depletion. This is most probably caused by the production of oxygen vacancies at the anode due to oxidation of the Cu electrode during DC polarization. Moreover the high field leads to onset of fast grain boundary diffusion in the entire sample. However, in contrast to similar perovskite-type oxides these changes are not accompanied by strong resistance degradation, probably due to the much lower oxygen vacancy concentrations.

Acknowledgement

Financial support by Christian Doppler Laboratory of Ferroic Materials is gratefully acknowledged.

References

[1] B. Jaffe, W.R.J. Cook, H. Jaffe, In: J.P. Roberts, P. Popper, Editors, Academic Press, London and New York, 1971, pp. 1–315.
[2] Y.-M. Chiang, D.P. Birnie, W.D. Kingery, Physical Ceramics. Principles for Ceramic Science and Engineering, John Wiley & Sons, Inc., 1997.
[3] S. Rodewald, J. Fleig, J. Maier, J. Am. Ceram. Soc. 83 (8) (2000) 1969.
[4] M.T. Chentir, E. Bouyssou, L. Ventura, C. Anceau, J. Appl. Phys. 105 (2009) 061605.
[5] D.C. Lupascu, J. Rödel, Adv. Eng. Mater. 7 (10) (2005) 882.
[6] X.J. Lou, J. Appl. Phys. 105 (024101) (2009) 1.
[7] P.J. Schorn, D. Bräuhaus, U. Böttger, R. Waser, G. Beitel, N. Nagel, R. Bruchhaus, J. Appl. Phys. 99 (2006) (114104)1.
[8] J.M. Liu, Y. Wang, C. Zhu, G.L. Yuan, S.T. Zhang, Appl. Phys. Lett. 87 (2005) 042904.
[9] R. Waser, T. Baiatu, K.H. Hardtl, J. Am. Ceram. Soc. 73 (6) (1990) 1645.
[10] Y. Genenko, J. Glaum, O. Hirsch, H. Kungl, M. Hoffmann, T. Granzow, Phys. Rev. B 80 (2009) 224109.
[11] D. Dimos, H. AlShareef, W. Warren, B. Tuttle, J. Appl. Phys. 80 (1996) 1682.
[12] S. Zhao, S.J. Zhang, W. Liu, N.J. Donnelly, Z. Xu, C.A. Randall, J. Appl. Phys. 105 (2009) 053705.
[13] R.-A. Eichel, Phys. Chem. Chem. Phys. 13 (2011) 368.
[14] R.A. De Souza, V. Metlenko, D. Park, T.E. Weirich, Phys. Rev. B 85 (2012) 174109.
[15] T. Frömling, H. Hutter, J. Fleig, J. Am. Ceram. Soc. 95 (2012) 1692.
[16] T. Frömling, H. Hutter, C. Leach, N. Ali, K. Reichmann, J. Fleig, Solid State Ionics 225 (2012) 727.
[17] E. Völkl, P. Hillebrand, J. Fleig, J. Electroceram. 27 (2011) 66.
[18] L. Andrejs, J. Fleig, J. Eur. Ceram. Soc. 33 (3) (2013) 779.
[19] G. Holzlechner, M. Kubicek, H. Hutter, J. Fleig, J. Anal. At. Spectrom. 28 (2013) 1080.
[20] M. Kubicek, G. Holzlechner, A. Opitz, S. Larisegger, H. Hutter, J. Fleig, Appl. Surf. Sci. (2013)(submitted for publication).
[21] J. Crank, The Mathematics of Diffusion, Second ed. Oxford Science Publication, 1975.
[22] R.T.P. Whipple, Philos. Mag. 45 (1954) 1225.
[23] A.D.L. Claire, Br. J. Appl. Phys. 14 (1963) 351.
[24] M. Hammer, M.J. Hoffmann, J. Am. Ceram. Soc. 81 (1998) 3277.
[25] R.D. Souza, J. Fleig, J. Maier, O. Kienzle, Z. Zhang, W. Sigle, M. Rühle, J. Am. Ceram. Soc. 86 (2003) 922.
[26] J. Maier, Physical Chemistry of Ionic Materials – Ions and Electrons in Solids, John Wiley & Sons, 2004.
[27] T. Frömling, A. Schintlmeister, H. Hutter, J. Fleig, J. Am. Ceram. Soc. 94 (2011) 1173.
[28] C. Slouka, L. Andrejs, J. Fleig, submitted for publication (2013).